ELSEVIER

J. Non-Newtonian Fluid Mech. 130 (2005) 110–116

Journal of Non-Newtonian Fluid Mechanics

www.elsevier.com/locate/jnnfm

Transient solutions of the dynamics in low-speed fiber spinning process accompanied by flow-induced crystallization

Joo Sung Lee, Dong Myeong Shin, Hyun Wook Jung *, Jae Chun Hyun

Department of Chemical and Biological Engineering, Applied Rheology Center, Korea University, Seoul 136-701, Republic of Korea

Received 12 June 2004; received in revised form 6 June 2005; accepted 1 August 2005

Abstract

The transient solutions of the fiber spinning process when flow-induced crystallization occurs on the spinline have not been reported yet in the literature. By contrast, the steady state behavior is well understood and has been simulated by many researchers, as has the transient behavior with no crystallization on the spinline. In this study, this particular issue has been investigated in the low-speed spinning case where no necklike deformation occurs on the spinline, incorporating flow-induced crystallization into the mathematical model of the system and then devising proper numerical schemes to produce temporal pictures of fiber spinning process. It turns out that the difficulty in obtaining transient solution for fiber spinning when it is accompanied by flow-induced crystallization lies in the extreme sensitivity of the spinline velocity toward the fluid stress level. This parameter plays a key role in finding the spinneret stress level for the numerical marching scheme employed in obtaining the solutions of the governing equations. This is in sharp contrast to the case of no crystallization on the spinline where the profiles of spinline variables are almost insensitive to the spinneret stress level, thus allowing previous researchers to obtain transient solutions with little difficulty. In addition to the successful transient solutions of fiber spinning dynamics with flow-induced crystallization reported in the present study, it is also shown that the destabilizing effect of flow-induced crystallization in low speed spinning process is confirmed by a linear stability analysis.

Keywords: Draw resonance; Fiber spinning; Flow-induced crystallization; Stability; Transient solutions

1. Introduction

The dynamics of fiber spinning, particularly that of melt spinning, has been studied by many research groups throughout the world during the last four decades since the first efforts by Kase and Matsuo [1] and Ziabicki [2] opened the realm. The stability, steady state process sensitivity, and various other aspects of the spinning dynamics have steadily attracted researchers' interest both in academia and industry, resulting in a voluminous body of information accumulated on the process [3–11]. Especially, the interesting instability phenomenon called draw resonance, frequently observed in fiber spinning (e.g., Liu and Beris [7] and Jung et al. [11]) along with in film casting (e.g., Iyengar and Co [12] and Lee et al. [13]) and film blowing (e.g., Yoon and Park [14] and Hyun et al. [15]), has been responsible for many important research results [7–15] ever since it was first experimentally observed and named as such in the early 1960s [16,17]. This draw resonance instability, a Hopf bifurcation instability, is not only an academically interesting stability subject but also an industrially important productivity issue.

Transient simulation of fiber spinning has naturally become an important subject as steady state solutions of the process had been readily available solving a set of governing partial differential equations covering various dynamics occurring in fiber spinning. Unfortunately, however, this transient solution has turned out extremely difficult to obtain if flow-induced crystallization (FIC) occurs on the spinline, while it is rather a simple exercise without it. To our knowledge, there has been no transient solution reported in the open literature when flow-induced crystallization is involved.

We have thus addressed this problem, i.e., obtaining transient solutions when flow-induced crystallization occurs on the spinline, since it is indispensable to developing strategies for stabilization and optimization of fiber spinning process [18]. Resolving the problem is equally warranted in other important polymer processing operations such as film casting [19] and film blowing [20,21] where the same flow-induced crystalliza-

* Corresponding author. Tel.: +82 2 3290 3306; fax: +82 2 926 6102.
E-mail address: hwjung@grtrkr.korea.ac.kr (H.W. Jung).

0377-0257/$ – see front matter © 2005 Elsevier B.V. All rights reserved.
doi:10.1016/j.jnnfm.2005.08.004

tion plays a crucial role in shaping their dynamics of extensional deformation.

2. Modeling

A nonisothermal model with crystallization kinetics was used in this study to obtain transient response of the spinning process whose schematic is shown in Fig. 1. A Phan-Thien–Tanner (PTT) constitutive equation, known for its robustness and accuracy in describing extensional deformation processes, was employed as a viscoelastic fluid model [22]. A one-phase crystallization model was adopted for the spinline fluid similar to those used by other researchers like Joo et al. [23], and Patel et al. [24], and the simulation for low speed spinning was conducted, where the nonlinear behavior called the spinline necking is absent. The two-phase crystallization model that handles the amorphous and crystalline phases in the fluid separately and is thus considered suitable for simulating high speed spinning with the necking, as eloquently described by Kulkarni and Beris [25], and Doufas et al. [26,27], was thus not employed in this study.

Equation of continuity:

$$\frac{\partial A}{\partial t^*} + \frac{\partial (AV)}{\partial Z} = 0. \tag{1}$$

Equation of motion:

$$\rho A \left(\frac{\partial V}{\partial t^*} + V \frac{\partial V}{\partial Z} \right) = \frac{\partial (A\sigma)}{\partial Z} + \rho g A - 2F_D \sqrt{\pi A}, \tag{2}$$

where $F_D = \frac{\rho_f V^2}{2} C_f$, $C_f = 0.65 \left(\frac{2V\sqrt{A}}{\nu_f \sqrt{\pi}} \right)^{-0.81}$.

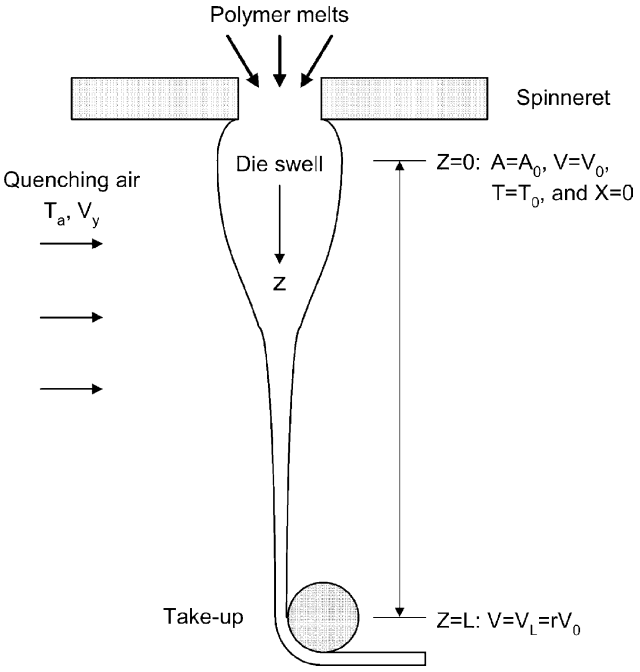

Fig. 1. Schematic diagram of fiber spinning process.

Constitutive equation (PTT fluids):

$$K^*\sigma + \lambda \left[\frac{\partial \sigma}{\partial t^*} + V \frac{\partial \sigma}{\partial Z} - 2(1-\xi)\sigma \frac{\partial V}{\partial Z} \right] = 2G\lambda \frac{\partial V}{\partial Z}, \tag{3}$$

where $K^* = \exp\left[\frac{\varepsilon\sigma}{G}\right]$, $\eta = \eta_0 \exp\left[\frac{E_a}{R}\left(\frac{1}{T} - \frac{1}{T_0}\right) + \alpha \frac{X}{X_\infty}\right]$, $G = G_0 \exp\left[3.2 \frac{X}{X_\infty}\right]$,

$$\lambda = \frac{\eta}{G} = \lambda_0 \exp\left[\frac{E_a}{R}\left(\frac{1}{T} - \frac{1}{T_0}\right) + (\alpha - 3.2)\frac{X}{X_\infty}\right].$$

Equation of energy:

$$\frac{\partial T}{\partial t^*} + V \frac{\partial T}{\partial Z} = -\frac{2\sqrt{\pi}h}{\rho C_p \sqrt{A}}(T - T_a) + \frac{\Delta H_f^*}{C_p}\left(\frac{\partial X}{\partial t^*} + V \frac{\partial X}{\partial Z} \right), \tag{4}$$

where $h = 0.473 \times 10^{-4} \left(\frac{V}{A}\right)^{1/3} \left[1 + \left(8 \frac{V_y}{V}\right)^2\right]^{1/6}$.

Crystallinity equation:

$$\frac{\partial X}{\partial t^*} + V \frac{\partial X}{\partial Z} = n \left[\ln\left(\frac{X_\infty}{X_\infty - X} \right) \right]^{\frac{n-1}{n}} (X_\infty - X) K_{max} \times \exp\left[-4 \ln 2 \left(\frac{T - T_{max}}{D} \right)^2 + \kappa \left(\frac{\sigma}{G_0} \right) \right]. \tag{5}$$

Boundary conditions:

$$A = A_0, \quad V = V_0, \quad T = T_0, \quad X = 0, \quad \text{at } Z = 0 \quad \text{and} \quad t^* \geq 0, \tag{6a}$$

$$V = V_L = rV_0, \quad \text{at } Z = L \quad \text{and} \quad t^* = 0, \tag{6b}$$

$$V = V_L = rV_0(1 + \delta), \quad \text{at } Z = L \quad \text{and } t^* > 0, \tag{6c}$$

where A is the spinline cross-sectional area, V the spinline velocity, t^* the elapsed time, Z the spatial coordinate in the flow direction, ρ the fluid density, L the spinning distance, σ the fluid axial extra stress, g the gravity acceleration constant, F_D the air-drag per unit surface area, C_f the friction coefficient, ρ_f the air density, ν_f the kinematic viscosity of the air, λ the fluid relaxation time, ε and ξ the PTT model parameters, η the fluid shear viscosity, G the fluid shear modulus, α the model parameter representing the crystallinity dependency of the viscosity, T the fluid temperature, T_a the cooling air temperature, C_p the fluid heat capacity, h the heat transfer coefficient between the fluid and the cooling air, V_y the cooling air velocity, ΔH_f^* the crystallization heat, X the crystallinity, X_∞ the ultimate crystallinity, n the Avrami index, K_{max} the maximum crystallization rate, T_{max} the fluid temperature having the maximum crystallization rate, D the crystallization half width temperature range, κ the flow-induced crystallization (FIC) enhancement factor representing the stress dependency of the crystallization rate following the similar models in the literature [26,27], r the drawdown ratio, and δ is the constant step disturbance at take-up velocity. Subscripts 0 and L mean die exit and take-up conditions, respectively. It should be noted that the trace of extra stress tensor in the flow-induced

Table 1
Model parameters for iPP

Parameters	Values	Ref.
Density, ρ (kg/m^3)	970	[31]
Heat capacity, C_p (cal/(g °C))	0.46	[31]
Zero-shear viscosity, η_0 (Poise)	34200	[31]
Relaxation time, λ_0 (s)	0.04	[31]
PTT model parameters, ε and ξ	0.015, 0.6	[28]
Dimensionless activation energy, E/R (K)	5.602×10^3	[31]
Heat of crystallization, ΔH_f (J/g)	148.453	[31]
Maximum crystallization rate, K_{max} (s^{-1})	0.55	[2]
Temperature at max. crystallization rate, T_{max} (K)	338	[2]
Crystallization half width temperature range, D (K)	333	[2]
Maximum crystallinity, X_∞ (%)	55	[29]
Crystallinity dependency parameter of viscosity, α	5.1	[30]
Flow-induced crystallization enhancement factor, κ	8.2	[29]

term in the crystallinity equation is simply reduced to the single axial extra stress, σ, in our 1-D model [26].

In the present study, isotactic polypropylene (iPP) has been selected as an example fluid for spinning with flow-induced crystallization to compare with experimental results in the literature. Some of the rheological properties and model parameters capable of predicting the fundamental aspects of iPP are summarized in Table 1 [2,28–31]. The PTT model parameters for iPP resin were adopted from the literature considering the nature of its extension thinning behavior [28]. The flow-induced crystallization (FIC) enhancement factor, κ, which the spinline crystallinity profiles are acutely sensitive to, has taken on the value of 8.2 for iPP as determined from the experimental crystallinity data of Kolb et al. [29] as shown in Fig. 2(a). The simulated results then agree well with the experimental data of the spinline cross-section area profile by Kolb et al. [29] (Fig. 2(b)), confirming the reasonable choice of rheological parameters for iPP.

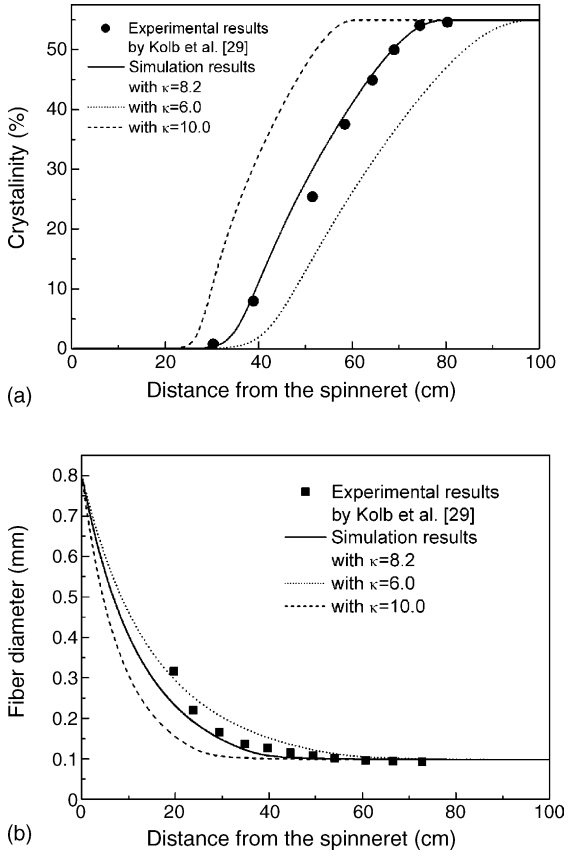

Fig. 2. Comparison of simulation results with experimental data [29] of (a) crystallinity and (b) fiber diameter for iPP fiber spinning at $r = 66.67$, $v_0 = 0.6$ m/min, $v_L = 40$ m/min, $\lambda_0 = 0.04$ s, $T_a = 25$ °C and $T_0 = 210$ °C to obtain the best value of FIC enhancement factor ($\kappa = 8.2$).

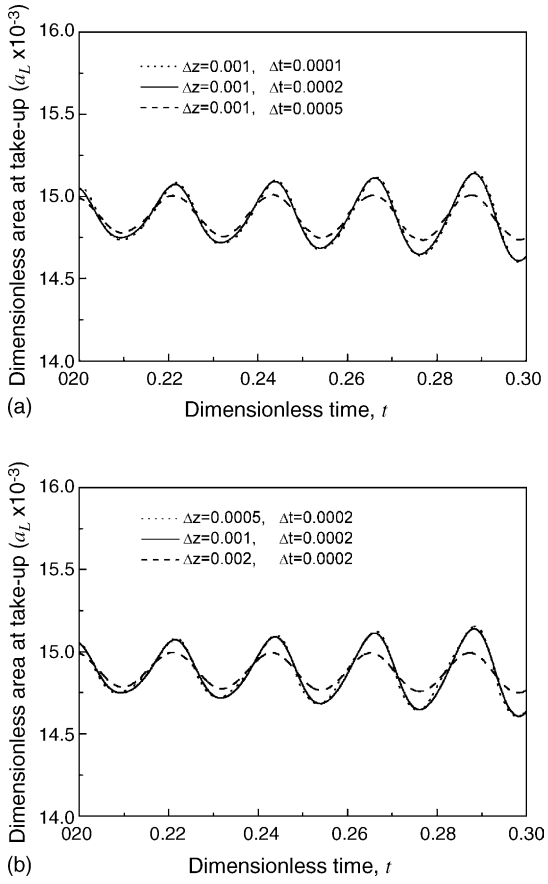

Fig. 3. Determination of optimal (a) temporal and (b) spatial mesh points for numerical simulation using the same conditions of Fig. 6(c).

Although many researchers have assumed the fluid modulus maintaining a constant value throughout the spinline based on the fact that the temperature dependency of the fluid modulus is much smaller than that of the shear viscosity. However, the crystallinity dependency of the fluid modulus turns out to be rather substantial as shown by Muslet and Kamal [30]. Their quite useful model for the fluid modulus, i.e., the function of crystallinity, has thus been adopted in this study as shown in Eq. (3). The fluid viscosity and the relaxation time are then the functions of temperature and crystallinity both, which consequently prevents an abnormal increase in the spinline stress, one of the main difficulties obtaining the transient solutions when flow-induced crystallization occurs on the spinline.

The dimensional equations of Eqs. (1)–(6) are now rendered into the following dimensionless form.

Equation of continuity:

$$\frac{\partial a}{\partial t} + \frac{\partial (av)}{\partial z} = 0, \tag{7}$$

where $a = \frac{A}{A_0}$, $v = \frac{V}{V_0}$, $t = \frac{t^* V_0}{L}$, $z = \frac{Z}{L}$.

Equation of motion:

$$C_{\text{in}} \left(\frac{\partial v}{\partial t} + v \frac{\partial v}{\partial z} \right) = \frac{1}{a} \frac{\partial (a\tau)}{\partial z} + C_{\text{gr}} - C_{\text{ad}} v^{1.19} a^{-0.905}, \tag{8}$$

where $C_{\text{in}} = \frac{\rho V_0 L}{2\eta_0}$, $C_{\text{gr}} = \frac{\rho g L^2}{2\eta_0 V_0}$,
$C_{\text{ad}} = \frac{3.122 \times 10^{-4} V_0^{0.19} L^2}{2 A_0^{0.905} \eta_0}$, $\tau = \frac{\sigma}{2\eta_0 V_0 / L}$.

Constitutive equation (PTT fluids):

$$K\tau + De \left[\frac{\partial \tau}{\partial t} + v \frac{\partial \tau}{\partial z} - 2(1-\xi)\tau \frac{\partial v}{\partial z} \right] = \frac{\eta}{\eta_0} \frac{\partial v}{\partial z}, \tag{9}$$

where $K = \exp\left[\frac{2\varepsilon De_0 \tau}{\exp(3.2x)}\right]$, $De = \frac{\lambda V_0}{L}$, $De_0 = \frac{\lambda_0 V_0}{L}$,

$$De = De_0 \exp\left[\frac{E_{\text{a}}}{RT_0} \left(\frac{1}{\theta} - 1 \right) + (\alpha - 3.2)x \right],$$

$$\eta = \eta_0 \exp\left[\frac{E_{\text{a}}}{RT_0} \left(\frac{1}{\theta} - 1 \right) + \alpha x \right].$$

Equation of energy:

$$\frac{\partial \theta}{\partial t} + v \frac{\partial \theta}{\partial z} = -St v^{1/3} a^{-5/6} (\theta - \theta_{\text{a}}) \left[1 + 64 \left(\frac{v_{\text{y}}}{v} \right)^2 \right]^{1/6} + \Delta H_{\text{f}} \left(\frac{\partial x}{\partial t} + v \frac{\partial x}{\partial z} \right), \tag{10}$$

where $St = \frac{1.67 \times 10^{-4} L}{\rho C_{\text{p}} V_0^{2/3} A_0^{5/6}}$, $\theta = \frac{T}{T_0}$,
$\theta_{\text{a}} = \frac{T_{\text{a}}}{T_0}$, $v_{\text{y}} = \frac{V_{\text{y}}}{V_0}$, $\Delta H_{\text{f}} = \frac{\Delta H_{\text{f}}^* X_\infty}{C_{\text{p}} T_0}$.

Crystallinity equation:

$$\frac{\partial x}{\partial t} + v \frac{\partial x}{\partial z} = n \left[\ln \left(\frac{1}{1-x} \right) \right]^{(n-1/n)} (1-x) k_m \times \exp\left[-4 \ln 2 \left(\frac{\theta - \theta_{\max}}{d} \right)^2 + 2\kappa \tau De_0 \right], \tag{11}$$

where $x = \frac{X}{X_\infty}$, $k_m = \frac{K_{\max} L}{V_0}$, $\theta_{\max} = \frac{T_{\max}}{T_0}$,
$d = \frac{D}{T_0}$.

Boundary conditions:

$$a_0 = 1, \quad v_0 = 1, \quad \theta_0 = 1, \quad x_0 = 0, \quad \text{at } z = 0 \quad \text{and} \quad t \geq 0, \tag{12a}$$

$$v_L = r, \quad \text{at } z = 1 \quad \text{and} \quad t = 0, \tag{12b}$$

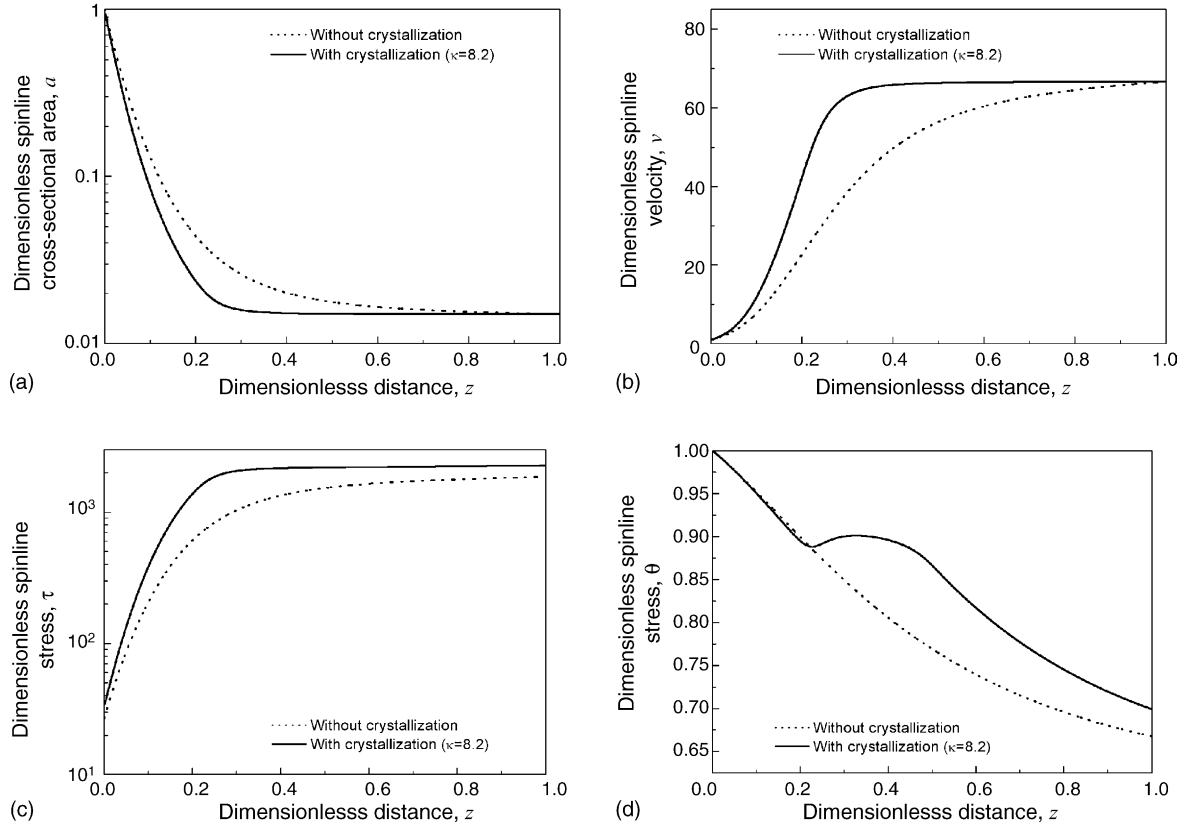

Fig. 4. Steady state spinline profiles obtained by simulation with and without crystallization for iPP fiber spinning at $r = 66.67$, $v_0 = 0.6$ m/min, $v_L = 40$ m/min, $\lambda_0 = 0.04$ s, $T_{\text{a}} = 25\,^\circ$C and $T_0 = 210\,^\circ$C.

$$v_L = r(1+\delta), \quad \text{at } z = 1 \quad \text{and} \quad t > 0. \tag{12c}$$

where a, v, t, z, and τ denote the dimensionless spinline cross-sectional area, spinline velocity, time, distance in the flow direction, and fluid axial extra stress, respectively, C_{in} the inertia coefficient, C_{gr} the gravity coefficient, C_{ad} the air-drag coefficient, De the Deborah number, St the Stanton number, and θ, θ_a, ΔH_f, v_y, x, k_m, θ_{max}, and d are the dimensionless spinline temperature, cooling air temperature, crystallization heat, cooling air velocity, crystallinity, maximum crystallization rate, temperature at maximum crystallization rate, and crystallization half width temperature range, respectively.

In this one-dimensional model, the radial variation of the stress is disregarded and the Avrami index, n, is set to unity because of the uniaxial extensional flow [25–27].

3. Numerical schemes

To solve the above governing equations, a finite difference method (FDM) was employed with 1000×5000 mesh points in z–t grid guaranteeing acceptable accuracy for the simulation results, because of the fact that only minimal improvements are gained as shown in Fig. 3 with smaller temporal and spatial mesh sizes than the optimal ones: the spatial coordinate being discretized by the backward difference method for the 2nd order accuracy, and for the time discretization, an absolutely stable 2nd order Gear method (so-called BDF2 method) being used to avoid numerical instabilities [32].

The extreme sensitivity of the spinline velocity toward the fluid stress level at spinneret, in sharp contrast to no-crystallization cases where the spinline velocity exhibits minimal sensitivity to the stress level at the spinneret, is found to be one reason for the difficulties obtaining the transient solutions of fiber spinning dynamics. A robust bracket method was used to resolve this matter as adopted in many optimization problems [33], to find precisely the initial stress level satisfying the velocity boundary conditions at take-up. After this initial stress guessing problem is overcome, there arises another in getting transient solutions especially when the system is in an oscillatory instability of draw resonance, mainly due to the very steep crystallinity profiles developed around the crystallization points on the spinline. To handle this difficulty, the governing equations have been solved in two steps, i.e., solving first the continuity, motion, constitutive and energy equations without the crystallinity equation using pre-guessed constant crystallinity values on the spinline initially adopted from the steady state solutions, and then solving next the full set of five equations using the improved values for the state variables generated by the first step as the starting values.

4. Results and discussions

According to the experimental results reported in the literature [18,20,29], the flow-induced crystallization occurs for iPP resins even at low speeds in fiber spinning and film casting. The spinline profiles of many state variables then exhibit very different shapes as compared with the no-crystallization cases as shown in Fig. 4, with the spinline velocity and the temperature increasing quite substantially triggered by spinline crystallization.

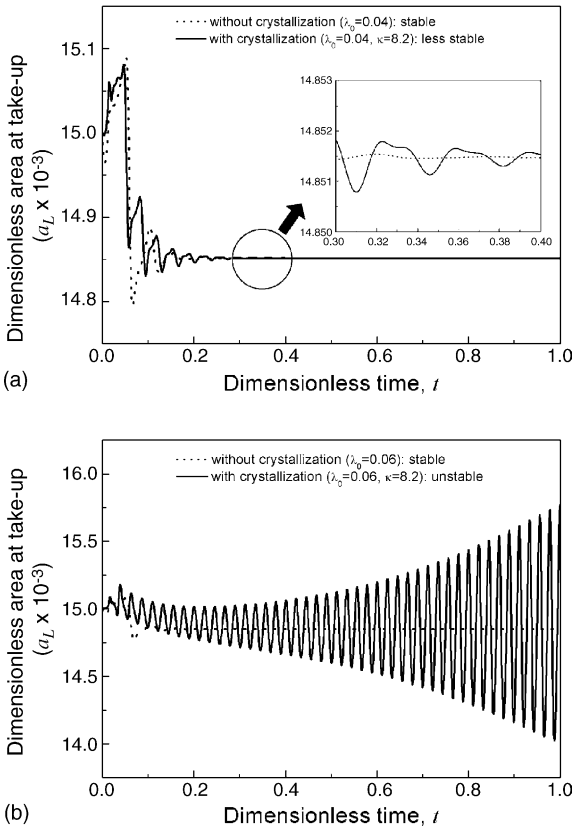

Fig. 5. Transient solutions for iPP fiber spinning with and without crystallization under the conditions (a) the same as in Fig. 4 and (b) the same as in Fig. 4 except for $\lambda_0 = 0.06$ s.

The transient solutions of the two cases of Fig. 4 with and without crystallization on spinline, have been obtained in this study when the 10% step change in take-up velocity (i.e., $\delta = 0.1$) is introduced, and then are displayed in Fig. 5. Although the both cases are stable, the case with crystallization emerges as less stable, taking more time converging to the steady state, revealing that the spinline crystallization destabilizes the iPP spinning process. Such destabilizing effect of the crystallization on the spinning has also been clarified by the linear stability analysis. (Appendix A shows the details about this linear stability analysis.) The real part of the leading eigenmode of the system with crystallization indeed shows the larger value than that without crystallization, i.e., -15.29 versus -26.79, confirming the less stable nature of the crystallization case.

Once the numerical schemes of this study prove capable of producing transient solutions of the spinning with spinline crystallization, other sensitivity studies can be easily performed as well. As Fig. 5(a and b) show, the destabilizing effect of the fluid viscoelasticity, which is characteristic of extension thinning fluids [13,28] including iPP in this study, is more pronounced when the crystallization occurs on the spinline. Also, the steady state spinline profile of crystallinity moves toward the spinneret with the increasing viscoelasticity as shown in Fig. 6(a). Fig. 6(b)

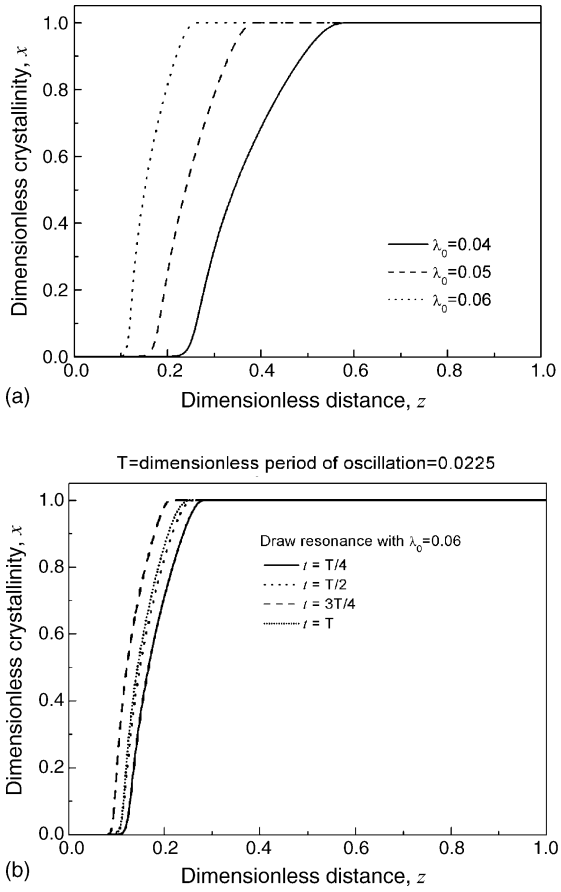

Fig. 6. Numerical solutions for iPP fiber spinning at $r = 66.67$, $v_0 = 0.6$ m/min, $v_L = 40$ m/min, $T_a = 25\,^{\circ}$C and $T_0 = 210\,^{\circ}$C: (a) steady profiles of spinline crystallinity with three different fluid relaxation times (viscoelasticity) and (b) one-cycle evolution of crystallinity profile during draw resonance instability with $\lambda_0 = 0.06$ s.

displays the one-cycle evolution of crystallinity profile when the system is in draw resonance under the conditions of Fig. 5(b). Fig. 7 shows the results of the linear stability analysis of the systems with crystallization (without crystallization, the system is found always stable as far as the operating conditions remain in the attainable region of the stability diagram), clearly demonstrating once again the less stable nature of the crystallization cases. More detailed stability results of spinning process when it is accompanied by flow-induced crystallization including high-speed spinning where neck-like deformation occurs, will be reported elsewhere later [34].

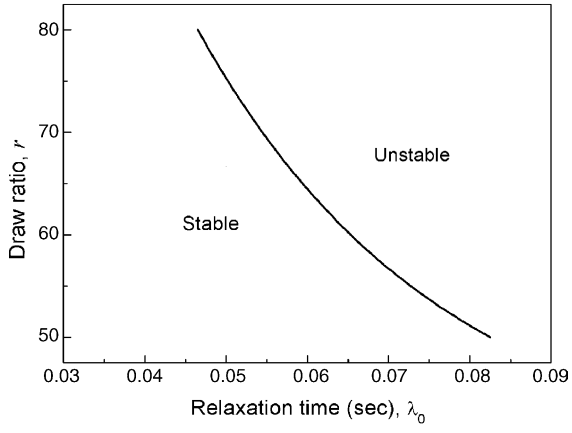

Fig. 7. Stability diagrams for the systems with crystallization produced by the linear stability analysis plotted against fluid relaxation time.

The above analysis of the effect of flow-induced crystallization on spinning dynamics and stability has only been possible with the transient solutions available. These transient solutions then make possible further stabilization and optimization strategies for spinning to improve the process productivity. The same approach should also be equally applicable to other extension deformation processes like film casting and film blowing processes for the same productivity improvements.

5. Conclusions

The transient solutions of fiber spinning process accompanied by flow-induced crystallization (FIC) have been obtained for the first time for low speed spinning, employing the model of the crystallinity-dependent fluid modulus as reported in the literature into the governing equations along with the newly devised numerical schemes. Isotactic polypropylene (iPP) was selected as an example fluid in this simulation study to compare with literature results. From the results of transient responses in fiber spinning with flow-induced crystallization available as reported in this study, it has been found that the low-speed spinning system is destabilized by crystallization on the spinline. Another theoretical tool, the linear stability analysis, exactly supports this finding. Utilizing the numerical techniques capable of producing transient solutions of this system, the stabilization and optimization of fiber spinning can be readily pursued using the information on the transient behavior of the process. The same approach is equally applicable to other extensional deformation polymer processings like film casting and film blowing.

Acknowledgements

This study was supported by research grants from the Korea Science and Engineering Foundation (KOSEF) through the Applied Rheology Center (ARC), an official KOSEF-created engineering research center (ERC) at Korea University, Seoul, Korea.

Appendix A

To briefly describe the linear stability analysis, the governing equations are compactly represented in a vector residual form.

$$\underline{R}(\underline{q},\ \dot{\underline{q}}) = \underline{0}. \tag{A.1}$$

where $\underline{q} = \underline{q}(\underline{a}, \underline{v}, \underline{\tau}, \underline{\theta}, \underline{x})$ is the state variable vector of spinline area, velocity, axial stress, temperature, and crystallinity. The vector $\dot{\underline{q}}$ denotes the time derivative of $\underline{q}$.

The temporal perturbations are then introduced into the state variables to get the following perturbation variables.

$$\underline{q}(t, z) = \underline{q}_S(z) + \delta\underline{q}(t, z). \tag{A.2}$$

where $\underline{\delta q}$ represents the perturbed quantities of states variables, and $\underline{q}_S$ is obtained from $\underline{R}(\underline{q}_S, \underline{0}) = \underline{0}$.

On substituting these perturbation variables into the governing equations, Eq. (A.1) is then linearized as follows.

$$\underline{\underline{J}}\,\underline{\delta q} - \underline{\underline{M}}\,\underline{\delta \dot{q}} = \underline{0}. \tag{A.3}$$

where $\underline{\underline{J}} \equiv \frac{\partial \underline{R}}{\partial \underline{q}}$, $\underline{\underline{M}} \equiv -\frac{\partial \underline{R}}{\partial \underline{\dot{q}}}$ are the Jacobian and mass matrices, respectively.

Next, after replacing $\underline{\delta q}(t, z)$ by $\underline{y}(z)\,e^{\Omega t}$, where Ω is a complex eigenvalue that accounts for the growth rate of the perturbation, and using a proper finite difference scheme, finally an eigenmatrix system is obtained.

$$\Omega \underline{\underline{M}}\,\underline{y} = \underline{\underline{J}}\,\underline{y} \tag{A.4}$$

The stability of the system is then determined by eigenvalues, Ω. If the real part of the dominant eigenvalue of Ω for a given condition is found positive, then the system is unstable, meaning that any initial disturbance introduced in the perturbation variables in Eq. (A.2) grows unbounded with time.

References

[1] S. Kase, T. Matsuo, Studies on melt spinning. I. Fundamental equations on the dynamics of melt spinning, J. Polym. Sci. Part A 3 (1965) 2541–2554.

[2] A. Ziabicki, Fundamentals of Fiber Formation, Wiley-Interscience, New York, 1976.

[3] J.R.A. Pearson, M.A. Matovich, Spinning a molten threadline: stability, Ind. Eng. Chem. Fundam. 8 (1969) 605–609.

[4] M.M. Denn, C.J.S. Petrie, P.A. Avenas, Mechanics of steady spinning of a viscoelastic liquid, AIChE J. 21 (1975) 791–799.

[5] J.L. White, Y. Ide, Instabilities and failure in elongational flow and melt spinning of fibers, J. Appl. Polym. Sci. 22 (1978) 3057–3074.

[6] A.N. Beris, B. Liu, Time-dependent fiber spinning equations. 1. Analysis of the mathematical behavior, J. Non-Newtonian Fluid Mech. 26 (1988) 341–361.

[7] B. Liu, A.N. Beris, Time-dependent fiber spinning equations. 2. Analysis of the stability of numerical approximation, J. Non-Newtonian Fluid Mech. 26 (1988) 363–394.

[8] D. Gelder, The stability of fiber drawing processes, Ind. Eng. Chem. Fundam. 10 (1971) 534–535.

[9] R.J. Fisher, M.M. Denn, A theory of isothermal melt spinning and draw resonance, AIChE J. 22 (1976) 236–246.

[10] J.C. Hyun, Theory of draw resonance. I. Newtonian fluids, AIChE J. 24 (1978) 418–422;
J.C. Hyun, Theory of draw resonance. II. Power-law and Maxwell fluids, AIChE J. 24 (1978) 423–426.

[11] H.W. Jung, H.-S. Song, J.C. Hyun, Draw resonance and kinematic waves in viscoelastic isothermal spinning, AIChE J. 46 (2000) 2106–2111.

[12] V.R. Iyengar, A. Co, Film casting of a modified Giesekus fluid: stability analysis, Chem. Eng. Sci. 51 (1996) 1417–1430.

[13] J.S. Lee, H.W. Jung, J.C. Hyun, Frequency response of film casting process, Kor. Aust. Rheol. J. 15 (2003) 91–96.

[14] K.-S. Yoon, C.-W. Park, Stability of a two-layer blown film coextrusion, J. Non-Newtonian Fluid Mech. 89 (2000) 97–116.

[15] J.C. Hyun, H. Kim, J.S. Lee, H.-S. Song, H.W. Jung, Transient solutions of the dynamics in film blowing processes, J. Non-Newtonian Fluid Mech. 121 (2004) 157–162.

[16] R.E. Christensen, Extrusion coating of polypropylene, SPE J. 18 (1962) 751–755.

[17] J.C. Miller, Swelling behavior in extrusion, SPE Trans. 3 (1963) 134–137.

[18] S.G. Hatzikiriakos, K. Migler (Eds.), Polymer Processing Instabilities: Control and Understanding, Marcel Dekker, New York, 2005.

[19] G. Lamberti, G. Titomanlio, Evidence of flow induced crystallization during characterized film casting process, Macromol. Symp. 185 (2002) 167–180.

[20] M.D. Bullwinkel, G.A. Campbell, D.H. Rasmussen, J. Krexa, C.J. Brancewitz, Crystallization studies of LLDPE during tubular blown film processing, Intern. Polym. Proc. 16 (2001) 39–47.

[21] D. Choi, J.L. White, Crystallization and orientation development in fiber and film processing of polypropylenes of varying stereoregular form and tacticity, Polym. Eng. Sci. 44 (2004) 210–222.

[22] N. Phan-Thien, A nonlinear network viscoelastic model, J. Rheol. 22 (1978) 259–283.

[23] Y.L. Joo, J. Sun, M.D. Smith, R.C. Armstrong, R.A. Brown, R.A. Ross, Two-dimensional numerical analysis of non-isothermal melt spinning with and without phase transition, J. Non-Newtonian Fluid Mech. 102 (2002) 37–70.

[24] R.M. Patel, J.H. Bheda, J.E. Spruiell, Dynamics and structure development during high-speed melt spinning of nylon 66. II. Mathematical modeling, J. Appl. Polym. Sci. 42 (1991) 1671–1682.

[25] J.A. Kulkarni, A.N. Beris, A model for the necking phenomenon in high-speed fiber spinning based on flow-induced crystallization, J. Rheol. 42 (1998) 971–994.

[26] A.K. Doufas, A.J. McHugh, C. Miller, Simulation of melt spinning including flow-induced crystallization. Part I. Model development and predictions, J. Non-Newtonian Fluid Mech. 92 (2000) 27–66.

[27] A.K. Doufas, A.J. McHugh, C. Miller, A. Immaneni, Simulation of melt spinning including flow-induced crystallization. Part II. Quantitative comparisons with industrial spinline data, J. Non-Newtonian Fluid Mech. 92 (2000) 81–103.

[28] W. Minoshima, J.L. White, J.E. Spruiell, Experimental investigation of the influence of molecular weight distribution on the rheological properties of PP melts, Polym. Eng. Sci. 20 (1980) 1166–1176.

[29] R. Kolb, S. Seifert, N. Stribeck, H.G. Zachmann, Simultaneous measurements of small- and wide-angle X-ray scattering during low speed spinning of poly(propylene) using synchrotron radiation, Polymer 41 (2000) 1497–1505.

[30] I.A. Muslet, M.R. Kamal, Computer simulation of the film blowing process incorporating crystallization and viscoelasticity, J. Rheol. 48 (2004) 525–550.

[31] R. Zheng, P.K. Kennedy, A model for post-flow induced crystallization: general equations and predictions, J. Rheol. 48 (2004) 823–842.

[32] M.O. Deville, P.F. Fischer, E.H. Mund, High-Order Methods for Incompressible Fluid Flow, Cambridge University Press, Cambridge, 2002, pp. 99–119.

[33] G.V. Reklaitis, A. Ravindran, K.M. Ragsdell, Engineering Optimization: Methods and Applications, John Wiley & Sons, Inc., New York, 1983, pp. 37–62.

[34] D.M. Shin, J.S. Lee, H.W. Jung, J.C. Hyun, Effects of the flow-induced crystallization on the stability in low- and high-spinning processes, Rheol. Acta (2005) submitted for publication.